

Acoustic Surface Evanescent Wave and its Dominant Contribution to Extraordinary Acoustic Transmission and Collimation of Sound

Yu Zhou, Ming-Hui Lu,[†] Liang Feng,^{*} Xu Ni, Yan-Feng Chen,[†] Yong-Yuan Zhu, Shi-Ning Zhu, and Nai-Ben Ming
*National Laboratory of Solid State Microstructures and Department of Materials Science and Engineering, Nanjing University,
 Nanjing, 210093, People's Republic of China*

(Received 24 August 2009; revised manuscript received 19 January 2010; published 23 April 2010)

We demonstrate both theoretically and experimentally the physical mechanism that underlies extraordinary acoustic transmission and collimation of sound through a one-dimensional decorated plate. A microscopic theory considers the total field as the sum of the scattered waves by every periodically aligned groove on the plate, which divides the total field into far-field radiative cylindrical waves and acoustic surface evanescent waves (ASEWs). Different from the well-known acoustic surface waves like Rayleigh waves and Lamb waves, ASEW is closely analogous to a surface plasmon polariton in the optical case. By mapping the total field, the experiments well confirm the theoretical calculations with ASEWs excited. The establishment of the concept of ASEW provides a new route for the integration of subwavelength acoustic devices with a structured solid surface.

DOI: [10.1103/PhysRevLett.104.164301](https://doi.org/10.1103/PhysRevLett.104.164301)

PACS numbers: 43.35.+d, 42.79.Dj, 73.20.Mf, 78.66.Bz

The interactions between matter and waves have been systematically investigated for centuries in natural materials. Recently, the study of matter-wave interactions has been further extended to artificial metamaterials in various realms such as electronics [1], optics [2,3], acoustics [4], and even plasmonics [5]. Among them, the surface plasmon polariton (SPP) has received a lot of attention because of its close relation with a number of intriguing optical phenomena, such as superlens [6], surface enhanced Raman scattering [7], and extraordinary optical transmission (EOT) [8], which have enormous potential applications in the next generation nanoscale optoelectronics. However, recent progress shows that other types of surface excitation mechanisms, such as creep waves [9,10] or cylindrical waves [11,12], also play equally important roles in subwavelength metallic nanostructures.

Because of the similarities between sound and light, the rapid development of optical metamaterials intrigues extensive studies of acoustic counterparts. Acoustic negative refraction [13] and birefractance [14] have been experimentally demonstrated in acoustic metamaterials. Extraordinary acoustic transmissions (EAT) through both one-dimensional (1D) and two-dimensional (2D) subwavelength acoustic gratings were demonstrated and investigated in both experiment and theory [15–18]. The physical origin of EAT is the coupling of collective surface Bloch modes and Fabry-Perot resonance [15,16] (this coupled mode is also called leaky surface guided mode [17]). Sound collimation was also achieved by engineering the acoustic surface modes [19], which is similar to the light beaming phenomenon supported by SPP [20].

However, the study on EAT so far is not comprehensive since its theory is usually based on a macroscopic viewpoint concerning a mode expansion of pressure field. In this Letter, we will for the first time experimentally and theoretically investigate the rich physics behind EAT and

sound collimation by considering microscopic scattering dynamics on a 1D acoustic subwavelength structure. In our microscopic description, we show that the total pressure field involves dynamic scattering processes of two types of waves: One is acoustic surface evanescent waves (ASEWs) bound to the interface of a periodically grooved subwavelength structure; the other is cylindrical waves (CWs) that radiate into far field. Experimental characterization of EAT and sound collimation supported by this structure validates our analytical microscopic theory.

Our sample is a steel plate with periodically imperforated grooves on both sides and a single slit at the center, as depicted in Fig. 1(a). The thickness of the plate and the period of the grooves are $H = 4$ mm and $d = 5$ mm, respectively. The width of the central slit and the grooves w , and the depth of the grooves h are both 0.5 mm. The transmission spectrum through the central slit of the sample was measured with an acoustic plane wave incidence [21]. EAT has been observed in the measured transmission spectrum as shown in Fig. 1(b). Within the range of the scanned frequencies (from 20 to 90 kHz), there are two resonance peaks located at $\lambda = 1.902d$ ($f = 36.07$ kHz) and $\lambda = 1.035d$ ($f = 66.28$ kHz), respectively. Finite element simulations have been implemented to model the corresponding intensity field distributions at two resonance frequencies as shown in Figs. 1(c) and 1(d), respectively. At $f = 36.07$ kHz, the acoustic field is strong inside the central slit but weak in the vicinities of the grooves [see Fig. 1(c)]. This indicates that the transmittance is barely affected by the periodicity of the grooves. Fabry-Perot resonance in a single aperture is responsible for EAT at this frequency [15]. However, at $f = 66.28$ kHz, the acoustic field is stronger around the grooves due to the excitation of ASEWs, as shown in Figs. 1(d) and 1(e). It is evident that the effect of ASEWs is dominant when the phases are matched (the periodicity of the grooves is close

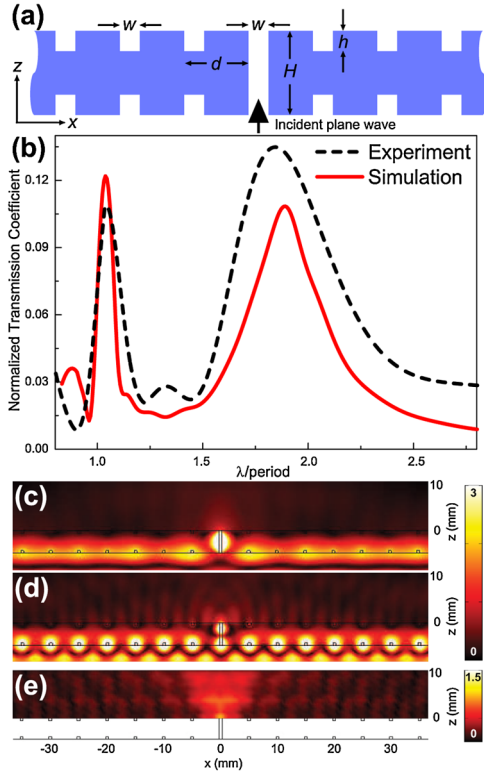


FIG. 1 (color online). (a) A schematic of the sample. There are $9 \times 4 = 36$ grooves in total; (b) Experimental (dashed-black line) and simulated (solid-red line) transmission spectra; (c) and (d) FEM simulated near-field intensity pattern in the vicinity of the sample at $\lambda = 1.902d$ and $\lambda = 1.035d$; (e) Experimental near-field intensity pattern in the vicinity of the sample at $\lambda = 1.035d$.

to the wavelength $\lambda = 1.035d$. The related frequency is denoted as the “resonance frequency” in the following text). It is worth noting that within the above experiment, two kinds of waves, ASEWs and radiative CWs, exist simultaneously. CWs are results of diffractions and scattering processes, while ASEWs are supported by the finite periodic subwavelength structure [22]. In order to understand the roles of these two different waves in the EAT and collimation effects, we developed a microscopic analytical method to calculate the transmission spectrum and the diffracted pressure field.

The central slit and the grooves can be treated as independent subwavelength cavities. Acoustic scattering depends only on the depth of the cavities and their geometric shapes. We first considered a more fundamental process in which waves are scattered by a cavity with infinite depth [23]. The transmission and reflection coefficients through this cavity are calculated using a Fourier modal method [24] with defining t_n , r_n , t_g , r_g as normal and grazing incidences from free space to cavity, respectively, and t_c , r_c as incidence from cavity to free space [Fig. 2(a)]. Because of boundary continuities, the expansions of the pressure and velocity fields of the fundamental cavity modes must match the plane wave expansions out-

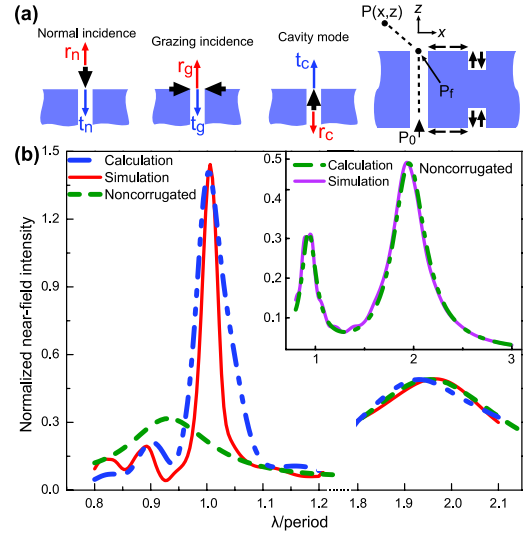


FIG. 2 (color online). (a) The left frames are schematics of the fundamental transmission and reflection coefficients defined in the first part of the calculation. The right frame is a schematic of the calculation process; (b) Calculated (dashed-blue line) and simulated (solid-red line) results of the normalized near-field intensity spectrum of the corrugated structure at $x = 0$ and $z = 2$ mm. Inset is a comparison of the noncorrugated structure.

side the cavity at the interface. Therefore, these coefficients under the condition of $w \ll \lambda$ can be expressed as $t_n = 2/(1 + G)$, $r_n = t_n - 1$, $t_g = F/(1 + G)$, $r_g = t_g - 1$, $r_c = (G - 1)/(G + 1)$, and $t_c = r_c + 1$, where $G = \frac{k_0}{\pi w} \int_{-\infty}^{+\infty} dQ \frac{1 - \cos(wQ)}{Q^2 \sqrt{k_0^2 - Q^2}}$, $F = \text{sinc} \frac{k_0 w}{2}$, and k_0 is the wave vector. Herein, G means the transmission properties of 1D single slit, originating from the coupling between the fundamental eigenmode and all diffractive waves [15,17]. Scattered pressure field of more complicated geometries, such as the slit and grooves in our experiments, can be calculated using these coefficients. With a normal incidence P_0 scattered by a cavity of depth H (or h), the pressure P_s at the center of the slit (or groove) on the interface can be expressed as $P_s = P_0(t_n r_c G_{\text{slit}} + r_n)$ for a slit, where $G_{\text{slit}} = t_c \exp(2ik_0 H)/[1 - \exp(2ik_0 H)r_c^2]$, and $P_s = P_0(t_n G_{\text{gv}} + r_n)$ for a groove, where $G_{\text{gv}} = t_c \exp(2ik_0 h)/[1 - \exp(2ik_0 h)r_c]$ (for details, see [21]).

The pressure P_s is regarded as a new point source and thus excites both CWs and ASEWs. For a CW that can propagate along the interface, its pressure field can be expressed as

$$P_{\text{CW}}(x) = P_s \cdot A_{\text{CW}}(x) = P_s \alpha_{\text{CW}} \exp(ik_0 x) \left(\frac{x}{\lambda}\right)^{-m}, \quad (1)$$

where α_{CW} is the scattering coefficient of the CW, $m \approx 0.5$ is the attenuation exponent of the CW [12], and k_0 is the propagation constant of sound in air. ASEW can also be excited if this series of periodic P_s on the surface are in phase and its expression is

$$P_{\text{ASEW}}(x) = P_s \cdot A_{\text{ASEW}}(x) = P_s \alpha_{\text{ASEW}} \exp(ik_{\text{ASEW}} x), \quad (2)$$

where α_{ASEW} is the scattering coefficient of the ASEW and

its propagation constant is

$$k_{\text{ASEW}} = k_0 \sqrt{1 + \left[\frac{w}{d} \tan(k_0 h) \right]^2}. \quad (3)$$

Since all scattered waves can only be funneled through the central slit, it is necessary to express the field inside the central slit. For simplicity, an assumption has been applied in calculation: All waves are scattered twice at most by the structure (this has turned out to be a good approximation for sound waves; however, multiscattering should be considered when dealing with EM waves.) The pressure field of the acoustic wave inside the central slit can be derived by combining Eqs. (1) and (2) with the fundamental transmission and reflection coefficients [see Fig. 2(a)]:

$$P_f = \left[P_0 t_n + 2t_g \sum_{n=1}^9 P_n A_{\text{tot}}(nd) \right] G_{\text{slit}} \exp(-ik_0 H), \quad (4)$$

where $A_{\text{tot}}(x) = A_{\text{ASEW}}(x) + A_{\text{CW}}(x)$, and P_n considers the contribution from the n th groove on the input side,

$$P_n = P_0(t_n G_{\text{gv}} + r_n) + (t_g G_{\text{gv}} + r_g) \left[P_0(t_n r_c G_{\text{slit}} + r_n) \times A_{\text{tot}}(nd) + \sum_{\substack{m=-9 \\ m \neq 0, n}}^9 P_0(t_n G_{\text{gv}} + r_n) A_{\text{tot}}(|m-n|) \right]. \quad (5)$$

Transmitted field through the central slit again excites CWs and ASEWs on the output interface, which can be calculated in a similar way. Since ASEWs are near-field waves, the transmitted pressure field mainly attributes to CWs (suppose $z = 0$ at the exit of the central slit):

$$P(x, z) = P_f A_{\text{CW}} \sqrt{x^2 + z^2} + \sum_{\substack{n=-9 \\ n \neq 0}}^9 P'_n A_{\text{CW}} \sqrt{(x-nd)^2 + z^2} \quad (6)$$

where P'_n is the contribution of the n th groove on the output interface (for details, see [21])

$$P'_n = P_f (t_g G_{\text{gv}} + r_g) A_{\text{tot}}(nd). \quad (7)$$

With our experimental configuration, the transmission spectrum of field intensity at $x = 0$ and $z = 2$ mm has been calculated and compared to the case in which there is only the central slit in the plate [see Fig. 2(b), P_0 normalized to 1). In these two different cases, the second peak almost remains the same, indicating a localized Fabry-Perot resonance without contribution from ASEWs, as shown in Fig. 1(c). At the first peak, however, the transmission is drastically enhanced (i.e., EAT is established) since the phase matching condition is satisfied and ASEWs are excited as seen in Figs. 1(d) and 1(e). According to Eqs. (4)–(7), although the near-field ASEWs can not directly contribute to the transmitted far field, they can modify the amplitude of CWs at the interface and affect the diffracted pattern of the far-field radiation.

To determine the relative weights of CWs and ASEWs in the total field, we analyzed the relation between ASEWs and CWs. From our calculation, it is shown that α_{ASEW} is

much smaller than α_{CW} ($\alpha_{\text{ASEW}} \approx 1/7\alpha_{\text{CW}}$ at the resonance frequency). This is different from the optical case, where SPP is the dominant factor [10,12]. But ASEWs can not be ignored because they barely decay with distance in our current length scale (a damping term $(\frac{x}{\lambda})^{-0.1}$ due to scattering from shallow grooves has been properly retrieved from simulations and added to Eq. (2) to precisely describe ASEWs' propagation). To demonstrate this, we calculated the pressure field distribution at $z = 0$ and $0 < x < 40$ mm at the resonance frequency using Eq. (6). At the input surface of the sample, ASEWs indeed directly contribute to the total field, so A_{CW} in Eq. (6) should be replaced by A_{tot} . As shown in Fig. 3, we found that field generated solely by the CWs does not agree with the simulation result; however, the total field including the contribution of ASEWs does. The phase matching condition is established for all the ASEWs generated by the grooves on the interface, resulting in a coherent transmission enhancement at the resonance frequency. Therefore, despite the fact that ASEWs have a relatively low weight in the total field, they are able to collect parts of the pressure from the grooves and funnel them through the central slit by modifying the amplitude of far-field radiative waves, which enhances the transmitted intensity many times larger than the case without grooves.

At the output side, the grooves act as radiators to effectively couple ASEWs to radiative waves in free space when the phases are matched. These radiators can slightly change the phase of ASEWs according to the position and depth of grooves, and thus modify the far-field diffracted patterns of the acoustic field [25]. Full range intensity field patterns at the resonance frequency have been mapped with an acoustic plane wave normally impinging on the sample, showing sound collimation in Fig. 4(a). The acoustic wave is well collimated after propagating $80\lambda_0$. This agrees well with simulations and calculations using our microscopic theory as shown in Figs. 4(b) and 4(c). We

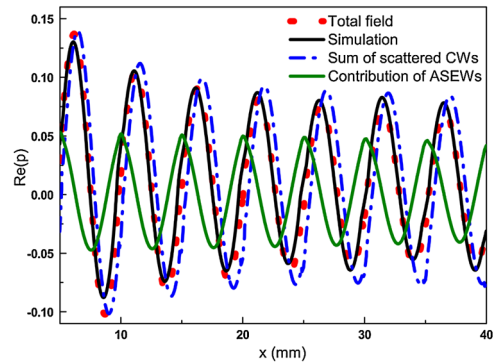


FIG. 3 (color online). Calculated pressure field on the right output side of the central slit ($z = 0$) at the resonance frequency. The total field (red dots, grey dots in the white-black line) is composed of the sum of all the CWs (dashed-dotted-blue line, black dashed-dotted blue line) and of the generated ASEWs (solid-green line, grey in the white-black line), and is compared with the simulated result (solid-black line).

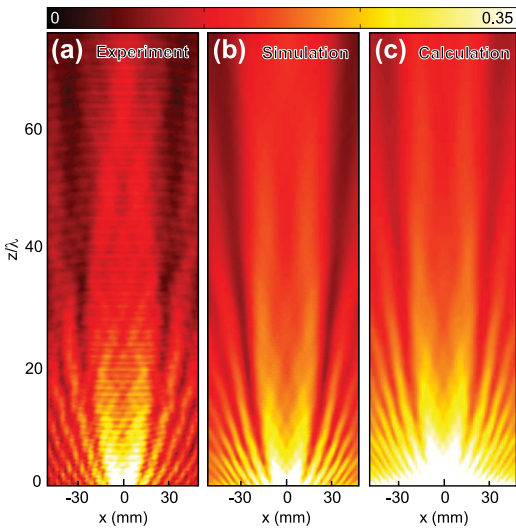


FIG. 4 (color online). (a) Experimental result of full-range intensity field pattern in the xz plane at the resonance frequency, showing the collimation effect; (b) Simulated intensity pattern at the resonance frequency. (c) Calculated intensity pattern at the resonance frequency using our microscopic theory.

also did calculations at other frequencies. However, such collimation effects are barely observable without excitation of ASEWs, which is consistent with our theoretical explanation.

In conclusion, we have experimentally observed and theoretically analyzed ASEWs and radiative CWs on the interface of our periodically grooved subwavelength structure as well as their associated EAT and sound collimation. More importantly, we have built a microscopic analytical model to describe the interaction between ASEWs and radiative CWs, which explains how ASEWs modulate and control far-field radiation by modifying the amplitudes of radiative waves. Although ASEW does not have a relatively high weight as SPP does in the optical case, it is still a key factor in both the EAT and sound collimation at the resonance frequency due to its impact on radiative CWs. These two kinds of waves make a contribution together and lead to novel acoustic effects [15–19,26–28] as well as potential acoustic devices and applications.

The work was jointly supported by the National Basic Research Program of China (Grant No. 2007CB613202) and the National Nature Science Foundation of China (Grant No. 50632030). We also acknowledge the support from the Changjiang Scholars, the Nature Science Foundation of China (Grant No. 10804043), and of Jiangsu Province (Grant No. BK2009007).

*Present address: Department of Electrical and Computer Engineering, University of CA, San Diego, CA 92093, USA.

†To whom correspondence should be addressed: luminghui@nju.edu.cn; yfchen@nju.edu.cn

- [1] J. B. Pendry, *Science* **315**, 1226 (2007).
- [2] R. A. Shelby, D. R. Smith, and S. Schultz, *Science* **292**, 77 (2001).
- [3] J. Valentine, S. Zhang, T. Zentgraf, E. Ulin-Avila, D. A. Genov, G. Bartal, and X. Zhang, *Nature (London)* **455**, 376 (2008).
- [4] Z. Y. Liu, X. X. Zhang, Y. W. Mao, Y. Y. Zhu, Z. Y. Yang, C. T. Chan, and P. Sheng, *Science* **289**, 1734 (2000).
- [5] L. Feng, M. H. Lu, V. Lomakin, and Y. Fainman, *Appl. Phys. Lett.* **93**, 231105 (2008).
- [6] X. Zhang and Z. W. Liu, *Nature Mater.* **7**, 435 (2008).
- [7] Y. Fang, N. H. Seong, and D. D. Dlott, *Science* **321**, 388 (2008).
- [8] T. W. Ebbesen, H. J. Lezec, H. F. Ghaemi, T. Thio, and P. A. Wolff, *Nature (London)* **391**, 667 (1998).
- [9] C. Genet and T. W. Ebbesen, *Nature (London)* **445**, 39 (2007).
- [10] P. Lalanne and J. P. Hugonin, *Nature Phys.* **2**, 551 (2006).
- [11] G. Gay, O. Alloschery, B. V. D. Leseugno, C. O'dwyer, J. Weiner, and H. J. Lezec, *Nature Phys.* **2**, 262 (2006).
- [12] X. Y. Yang, H. T. Liu, and P. Lalanne, *Phys. Rev. Lett.* **102**, 153903 (2009).
- [13] S. Zhang, L. L. Yin, and N. Fang, *Phys. Rev. Lett.* **102**, 194301 (2009).
- [14] M. H. Lu, C. Zhang, L. Feng, J. Zhao, Y. F. Chen, Y. W. Mao, J. Zi, Y. Y. Zhu, S. N. Zhu, and N. B. Ming, *Nature Mater.* **6**, 744 (2007).
- [15] M. H. Lu, X. K. Liu, L. Feng, J. Li, C. P. Huang, Y. F. Chen, Y. Y. Zhu, S. N. Zhu, and N. B. Ming, *Phys. Rev. Lett.* **99**, 174301 (2007).
- [16] B. Hou, J. Mei, M. Z. Ke, Z. Y. Liu, J. Shi, and W. J. Wen, *J. Appl. Phys.* **104**, 014909 (2008).
- [17] J. Christensen, L. Martín-Moreno, and F. J. García-Vidal, *Phys. Rev. Lett.* **101**, 014301 (2008).
- [18] J. Mei, B. Hou, M. Z. Ke, S. S. Peng, H. Jia, Z. Y. Liu, J. Shi, W. J. Wen, and P. Sheng, *Appl. Phys. Lett.* **92**, 124106 (2008).
- [19] J. Christensen, A. I. Fernandez-Dominguez, F. de Leon-Perez, L. Martín-Moreno, and F. J. García-Vidal, *Nature Phys.* **3**, 851 (2007).
- [20] N. F. Yu, J. Fan, Q. J. Wang, C. Pflügl, L. Diehl, T. Edamura, M. Yamanishi, H. Kan, and F. Capasso, *Nat. Photon.* **2**, 564 (2008).
- [21] See supplementary material at <http://link.aps.org/supplemental/10.1103/PhysRevLett.104.164301> for detailed elucidation of the analytical model and the schematic of the experiment setup.
- [22] L. Kelders, J. F. Allard, and W. Lauriks, *J. Acoust. Soc. Am.* **103**, 2730 (1998).
- [23] P. Lalanne, J. P. Hugonin, and J. C. Rodier, *Phys. Rev. Lett.* **95**, 263902 (2005).
- [24] Y. Takakura, *Phys. Rev. Lett.* **86**, 5601 (2001).
- [25] D. R. Matthews, H. D. Summers, K. Njoh, S. Chappell, R. Errington, and P. Smith, *Opt. Express* **15**, 3478 (2007).
- [26] H. Estrada, P. Candelas, A. Uris, F. Belmar, F. J. García Abajo, and F. Meseguer, *Phys. Rev. Lett.* **101**, 084302 (2008).
- [27] J. Christensen, P. A. Huidobro, L. Martín-Moreno, and F. J. García-Vidal, *Appl. Phys. Lett.* **93**, 083502 (2008).
- [28] M. Z. Ke, Z. J. He, S. S. Peng, Z. Y. Liu, J. Shi, W. J. Wen, and P. Sheng, *Phys. Rev. Lett.* **99**, 044301 (2007).